Pure Appl. Geophys. 174 (2017), 2561–2579

DOI 10.1007/s00024-017-1576-0

Pure and Applied Geophysics

Regional Seismic Intensity Anomalies in the Korean Peninsula and Its Implications for Seismic-Hazard Potentials

Seongjun Park [1] and Tae-Kyung Hong[1]

Abstract—The strength of seismic ground motion is a consequence of seismic source strength and medium response. The dependence of seismic amplitudes and seismic intensity on regional geological structures and crustal properties in the stable intraplate region around the Korean Peninsula is investigated. An instrumental seismic intensity scale based on spectral accelerations are proposed after calibrating with the reported macroseismic intensities. A representative seismic intensity attenuation curve for the Korean Peninsula is given by $I(M_L, l, h) = -0.998(\pm 0.222) + 1.72(\pm 0.04)M_L - 0.322(\pm 0.027) \ln(l^2 + h^2) - 0.00608 (\pm 0.00049)\sqrt{l^2 + h^2}$, where $I(M_L, l, h)$ is the seismic intensity at an epicentral distance l in km for an earthquake with local magnitude M_L and focal depth h in km. Seismic intensities decay slowly with distance in the Korean Peninsula. The observed decay rate for the Korean Peninsula is comparable with those for other stable intraplate regions, while are lower than those for active regions. The regional seismic intensity anomalies present a characteristic correlation with geological structures. Positive seismic intensity anomalies appear in the Yeongnam massif, Okcheon belt and Gyeongsang basin, while negative seismic intensity anomalies in the Gyeonggi massif. The regional seismic intensity anomalies display positive correlations with crustal thicknesses, crustal amplifications, and seismicity density and negative correlations with heat flows. Positive seismic intensity anomalies are observed in the Yeongnam massif and Gyeongsang basin, suggesting high seismic-hazard potentials in the regions. The regional crustal properties may provide useful information on potential seismic hazards.

Key words: Seismic hazards, Korean Peninsula, seismic intensity, crustal properties.

1. Introduction

Seismic damage generally increases with the level of seismic ground motions for the same vulnerability. The seismic ground motions are controlled by source strength, medium properties and distance. Seismic intensity is useful for intuitive recognition of the level of seismic damage or hazard (e.g., Slejko et al. 1998; Davenport 2001). The seismic intensity scalings have been widely applied for prompt seismic hazard assessment and prediction of seismic hazard risk (e.g., Cornell 1968; Slejko et al. 1998; Ardeleanu et al. 2005).

The seismic intensity generally increases with the strength of ground motion, and decreases with distance (e.g., Gupta and Nuttli 1973; Gasperini et al. 1999; Casado et al. 2000). The seismic intensity is suggested to be controlled by the frequency content as well as the strength of ground motion (e.g., Trifunac and Lee 1989; Sokolov and Chernov 1998). The influence of shallow medium on seismic intensities was understood limitedly (e.g., Borcherdt and Gibbs 1976; Tilford et al. 1985; Kawase and Aki 1990).

The seismic amplitudes and frequencies are affected by medium properties and source parameters, causing difference in seismic intensities at a common distance (Hanks and McGuire 1981; Geli et al. 1988; Chandler and Lam 2002; Hong and Kennett 2002). Thus, it is difficult to predict the seismic intensities without the knowledge of the regional variation of seismic intensities on regional structures (e.g., Hinzen and Oemisch 2001; Bakun and Scotti 2006; Zohar and Marco 2012).

We investigate the influence of regional-scale crustal properties on seismic intensities in the continental intraplate region around the Korean Peninsula. We introduce an instrumental seismic intensity scaling and determine the seismic intensities in the modified Mercalli intensity (MMI) scale from seismic ground motions. We investigate the correlations of

[1] Department of Earth System Sciences, Yonsei University, 50 Yonsei-ro, Seodaemun-gu, Seoul 120-749, South Korea. E-mail: tkhong@yonsei.ac.kr

Birkhäuser

regional seismic intensity anomalies between the seismic intensity anomalies and regional crustal properties.

2. Geology

The Korean Peninsula is located at the eastern margin of the Eurasian plate, which may be further divided into several tectonic provinces (e.g., Chough and Barg 1987; Heki et al. 1999; DeMets et al. 2010; Zhao et al. 2011). The Korean Peninsula is placed in an intraplate region at a distance of greater than 1000 km away from the nearest subduction zones around the Japanese islands (Fig. 1a).

Stresses originating from the convergent plate boundaries are transmitted into the lithosphere of the peninsula, constructing an intraplate regime with low seismicity dominated by strike-slip earthquakes (Hong and Choi 2012; Houng and Hong 2013). The occurrence rate of earthquakes with magnitudes greater than or equal to 3.0 are 8.43 year^{-1} (Hong et al. 2015). The national seismic seismic monitoring began in 1978. The largest event of which magnitude is M_L5.8 occurred in the southeastern Korean Peninsula on 12 September, 2016. According to historical literatures, the Korean Peninsula appears to have experienced earthquakes with magnitudes of $\sim$7.0 have occurred (Houng and Hong 2013; Hong et al. 2016).

The current shape of the geological provinces of the Korean Peninsula was formed by a series of orogenic events (Chough et al. 2000; Oh 2006). The orogeny may be associated with the paleo-collision between the North and South China blocks during late Permian to early Triassic and the subduction of a paleo oceanic plate during the early to late Jurassic (e.g., Yin and Nie 1993; Chang 1996; Chough et al. 2000; Oh 2006). The surface geology of the peninsula is composed of three precambrian massifs with high-grade gneisses and schists (Gyeonggi, Nangrim and Yeongnam massifs), two fold belts (Imjingang and Okcheon belts), a late Proterozoic to Phanerozoic basin (Pyeongnam basin), and a Cretaceous basin (Gyeongsang basin) (Fig. 1b). The complex geological setting constructs laterally heterogeneous crustal structures.

The crustal thicknesses in the Korean Peninsula are 28-38 km, which is typical in continental crusts (Chang and Baag 2007; Hong et al. 2008) (Fig. 2a). The East Sea (Sea of Japan) presents a transitional structure between continental and oceanic crusts with a seaward-decreasing crustal thickness reaching 8.5–14 km (Hirata et al. 1989; Kim et al. 2003; Hong et al. 2008). The Yellow Sea displays the properties of a continental crust, and the crustal thicknesses are close to those of the inland peninsula (Hong et al. 2008). The crustal thicknesses are relatively large in the western Gyeongsang basin, Yeongnam massif, and southern Gyeonggi massif, and are relatively small in the northern and western Gyeonggi massif.

The amplitudes of ground motions vary by geological structure (Hong and Lee 2012). We observe large seismic amplification in the Yeongnam massif and Gyeongsang basin, while low in the Gyeonggi massif (Fig. 2b). The *P* amplification is generally consistent with the shear-wave attenuation (Lg Q_0^{-1}) (Hong 2010; Jo and Hong 2013). A large shear-wave attenuation (Lg Q_0^{-1}) in the crust is found in the Yeongnam massif and Gyeongsang basin, and low attenuation is found in the central and southern Gyeonggi massif (Fig. 2c).

The spatial density of earthquakes (seismicity density) is high in the Okcheon belt, Yeongnam massif, and Gyeongsang basin, and low in the Gyeonggi massif (Fig. 2d). The seismicity densities appear to be correlated with the shear wave attenuation (Lg Q_0^{-1}) in most regions, which is consistent with other studies (Walsh 1966; Jin and Aki 1989; Main et al. 1990). This may be because medium heterogeneity is high in fault zones, which increases the seismic attenuation.

The surface heat flows reflect chemical composition of the crust and mantle (e.g., Helffrich and Wood 2001). The average surface heat flows in the Korean Peninsula is about 70 mW m^{-2} (Fig. 2e). We observe high heat flows in the western and eastern Gyeonggi massif and Gyeongsang basin. The Bouguer gravity anomalies appear to be generally correlated with the disposition of geological provinces (Cho et al. 1997; Jo and Hong 2013) (Fig. 2f). Positive Bouguer gravity anomalies are observed in the Gyeongsang basin, while negative anomalies are observed in the Gyeonggi massif, Okcheon belt and Yeongnam massif.

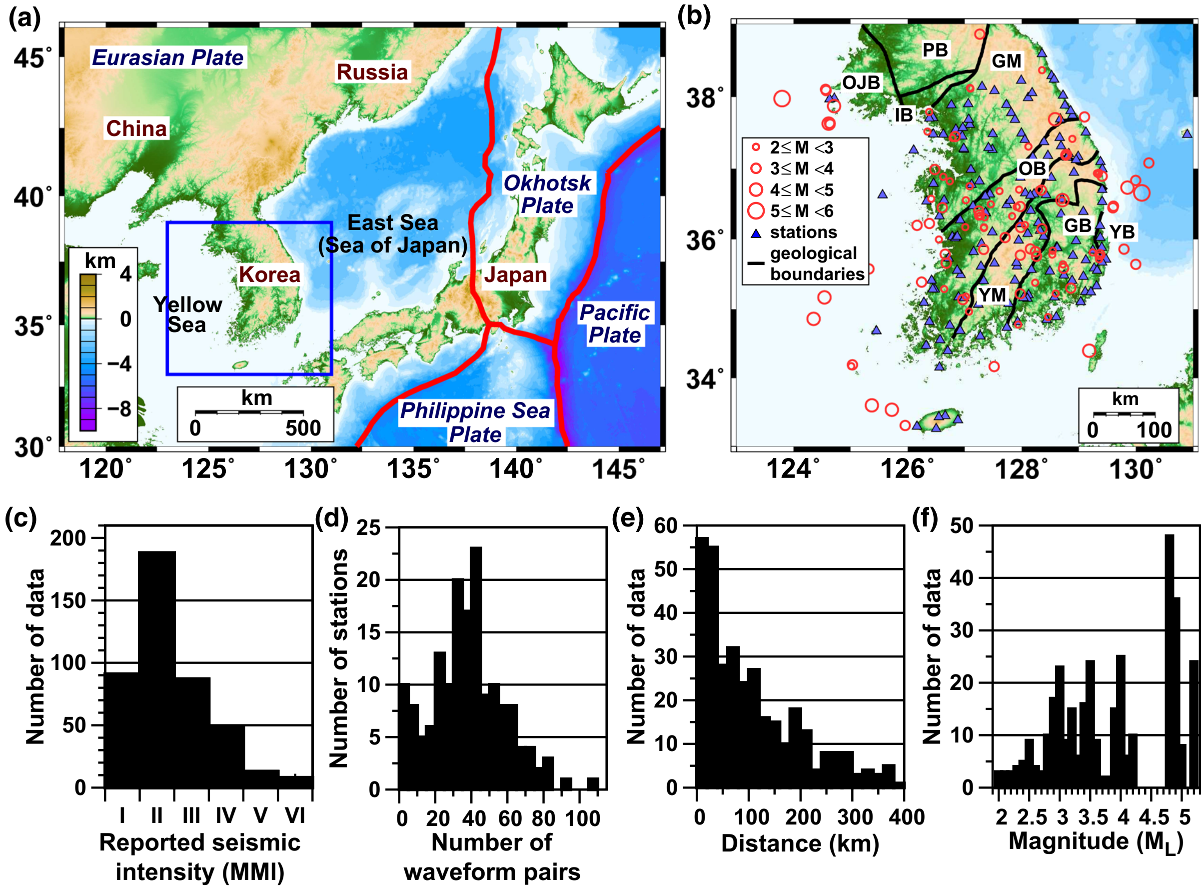

Figure 1

a Tectonic structures around the Korean Peninsula. The study area is marked with an *open rectangle*. **b** Distribution of seismic events (*open circles*) during 1978–2013 and stations (*filled triangles*) used in this study. The seismic stations are deployed densely over the peninsula. The major geological provinces in the Korean Peninsula are denoted as follows: *GM* Gyeonggi massif, *GB* Gyeongsang basin, *IB* Imjingang belt, *OB* Okcheon belt, *OJB* Ongjin basin, *PB* Pyeongnam basin, *YB* Yeonil basin, *YM* Yeongnam massif. **c** Distribution of reported macroseismic intensities for events during 2001–2013 (Korea Meteorological 2002, 2003, 2004, 2005, 2006, 2007, 2008, 2009, 2010, 2011, 2012, 2013, 2014). The total number of reported macroseismic intensities is 435. **d** Number of horizontal seismic-waveform pairs at each station. Distribution of waveform data with macroseismic intensities as a function of **e** distance and **f** magnitude

The average P velocity on the Moho is 7.95 km s^{-1}, which is lower than the global average of 8.05 km s^{-1} (Hong and Kang 2009) (Fig. 2g). The Moho-refracted P (Pn) velocities are high in the Gyeonggi massif, western Okcheon belt and western Gyeongsang basin, and are low in the eastern Okcheon belt, eastern Yeongnam massif and eastern Gyeongsang basin. However, the upper-crustal S velocities are high in the eastern Gyeonggi massif and Okcheon belt, and are low in the western Gyeonggi massif, Yeongnam massif, and Gyeongsang basin (Fig. 2h). The regional variations are different from those of the Pn velocities, suggesting differences in the physical and chemical properties between the upper and lower crusts (Choi et al. 2009; Jo and Hong 2013).

The P and S velocity ratio, V_P/V_S, can be converted into the Poisson ratio, representing a physical property of the rocks composing a medium (Jo and Hong 2013). High upper-crustal V_P/V_S ratios are found around the boundaries between the Gyeonggi massif and Okcheon belt, and between the Yeongnam massif and Okcheon belt (Jo and Hong 2013) (Fig. 2i). The V_P/V_S ratios present strong anti-correlation with the Pn velocities in most regions except the western Gyeonggi massif.

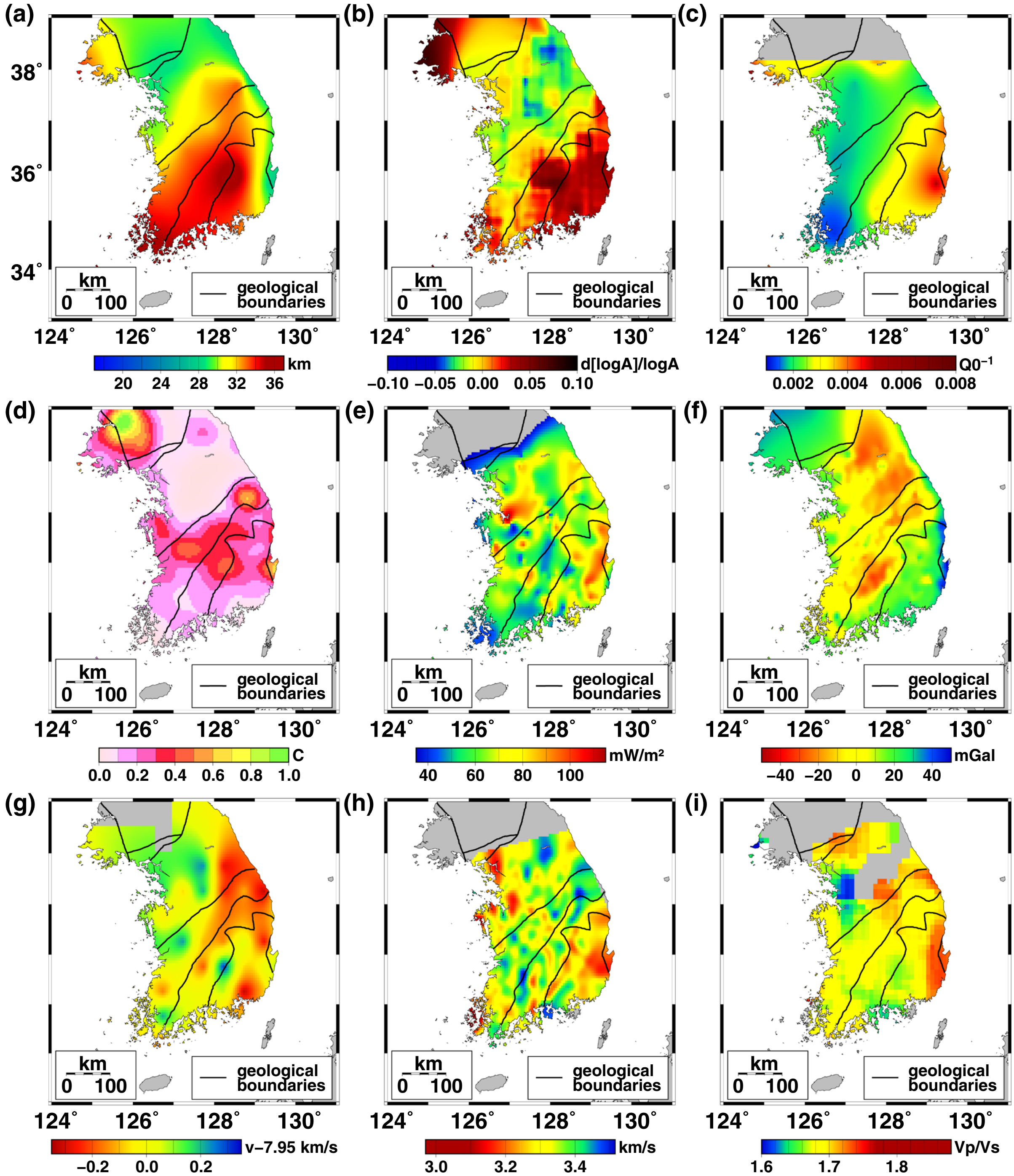

Figure 2
Regional variations in seismic and geophysical estimates in the Korean Peninsula: **a** crustal thicknesses (Hong et al. 2008), **b** crustal *P* amplification (Hong and Lee 2012), **c** crustally-guided shear-wave attenuations (Lg Q_0^{-1}) (Hong 2010), **d** seismicity densities, *C*, of earthquakes with magnitudes equal to or larger than 2.5 during 1978–2013 (Houng and Hong 2013), **e** surface heat flows (Lee et al. 2010), **f** Bouguer gravity anomalies (Cho et al. 1997), **g** variation in Moho *P* (Pn) velocities relative to 7.95 km s^{-1} (Hong and Kang 2009), **h** shear-wave velocities at a depth of 6.75 km (Choi et al. 2009), and **i** upper-crustal V_P/V_S ratios (Jo and Hong 2013)

3. Data

The Korea Institute of Geoscience and Mineral Resources (KIGAM) and the Korea Meteorological Administration (KMA) operate seismic networks that are densely deployed over the peninsula (Fig. 1b). The stations are equipped with three-component accelerometers (Kinemetrics ES-T and ES-DH and Guralp CMG-5T) of which sampling rates are 100 Hz. We collect 6016 pairs of horizontal accelerograms from 162 stations for 102 events during the period 2001–2013 (Figs. 1d, 3a, c). The stations are placed in the southern part of the Korean Peninsula (Fig. 3a). The event magnitudes (M_{L}) are 2.0–5.2, and the focal depths are 0.26–19.8 km.

The number of horizontal waveforms collected from each station ranges between 4 and 212 (Fig. 1d). We found 339 pairs of horizontal accelerograms that have reported macroseismic intensities (I^{rep}) (Fig. 1e, f). The number of waveform data generally decreases with distance, and increases with the event magnitude. These seismic waveforms are used in calibration of instrumental seismic intensity with respect to the reported macroseismic intensity.

The macroseismic intensities and source information of the earthquakes during the period 2001–2013 are available from the earthquake bulletins of KMA (available from http://www.kma.go.kr) and early studies (Korea Meteorological 2002, 2003, 2004, 2005, 2006, 2007, 2008, 2009, 2010, 2011, 2012, 2013, 2014; Kyung et al. 2007). We collect 435 macroseismic intensities in the MMI scale of 1–6 for the earthquakes during 2001-2013 with epicentral distances of 3–398 km (Figs. 1c, 3a, b). The reported macroseismic intensities decrease with distance, which is consistent with the amplitudes of ground motions (Fig. 3). The numbers of macroseismic intensities for earthquakes vary between 1 and 76 depending on the event strengths and event locations.

4. Theory

4.1. Instrumental Seismic Intensity

The seismic intensity may depend on the strength and duration of ground motion (Trifunac and Brady 1975; Hancock and Bommer 2006). The frequency content of ground motion is also an important parameter that controls the level of seismic intensity (e.g., Malhotra 1999; Snieder and Şafak 2006). Thus, the seismic intensity may be estimated from seismic waveforms. The spectral amplitudes of ground motions are useful for estimation of seismic intensity since they reflect the amplitudes, frequency contents and durations of ground motions (Sokolov and Chernov 1998). Note that the duration of ground motion is reflected through the size of the waveform window in calculation of seismic spectra. We analyze the instrumental seismic intensities for investigation of correlations with crustal properties.

The logarithmic spectral amplitudes of horizontal accelerations are proportional to the seismic intensity (Trifunac and Lee 1989). Thus, the instrumental seismic intensity can be written as

$$I = \sum_{i=1}^{Nf} w_i [k_1(f_i) \log A_{\mathrm{H}}(f_i) + k_2(f_i)], \qquad (1)$$

where I is the instrumental seismic intensity on the MMI scale, Nf is the number of discrete frequencies, f_i is the ith discrete frequency, $A_{\mathrm{H}}(f_i)$ is the spectral amplitude of horizontal acceleration at frequency f_i, w_i is the weighting factor accounting for the relative contribution of ground motion in frequency f_i to seismic intensity, and $k_1(f_i)$ and $k_2(f_i)$ are frequency-dependent constants.

The weighting factor w_i may vary by region according to medium properties that affect the frequency contents of ground motions. The weighting factors can be determined empirically based on the data set. Here, the spectral amplitude of horizontal acceleration, A_{H}, is determined by

$$A_{\mathrm{H}}(f) = \sqrt{\{A_{\mathrm{N}}(f)\}^2 + \{A_{\mathrm{E}}(f)\}^2}, \qquad (2)$$

where f is the frequency, A_{N} and A_{E} are the NS and EW spectral amplitudes in m s^{-1}.

The seismic intensity equation is further simplified for the analysis of spectral amplitudes in a narrow frequency band, assuming an uniform weighting factor:

$$I = k_1 \log \bar{S} + k_2, \qquad (3)$$

where k_1 and k_2 are constants, and $\bar{S}$ is the log-averaged A_{H} for an ascribed frequency band that is determined empirically. The constants k_1 and k_2 are determined by calibrating the estimated instrumental

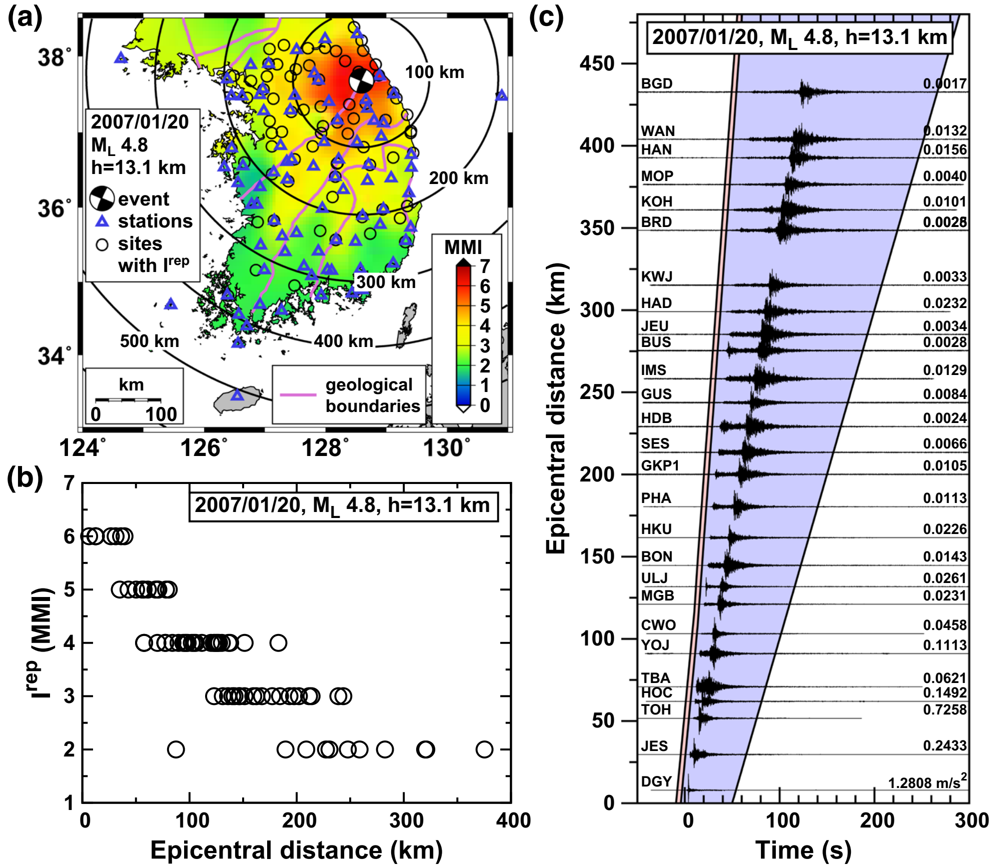

Figure 3

a Spatial variation in the reported macroseismic intensities (I^{rep}) for the 20 January 2007 $M_{\mathrm{L}}4.8$ earthquake with a focal depth (h) of 13.1 km. The sites of reported seismic intensities (*circles*) and locations of seismic stations (*triangles*) are marked. The focal mechanism solution of the event is presented (Kim and Park 2010; Kim et al. 2010; Hong and Choi 2012). Geological structures and equi-epicentral-distance contours are marked. **b** Variation of reported macroseismic intensities with distance. The reported macroseismic intensities generally decrease with distance. **c** The local and regional-distance accelerograms on the N–S component of the earthquake. The peak ground accelerations of the waveforms are denoted with the names of stations. The portion of wavetrains analyzed is shaded. The 5-s-long ambient noises before the first *P* arrivals used for the calculation of signal-to-noise ratios are marked

intensities with respect to the reported macroseismic intensities.

4.2. Seismic Intensity Attenuation with Distance

The seismic intensity is dependent on the source strength, medium properties and distance. The seismic intensity attenuates as a function of distance in uniform media. The seismic intensity at an epicentral distance of l for an event with magnitude M and focal depth h is given by (e.g., Bakun 2006; Pasolini et al. 2008)

$$I(M, l, h) = c + \alpha M - \beta \ln(R) - \gamma R, \qquad (4)$$

where R is the hypocentral distance ($= \sqrt{l^2 + h^2}$), and c, α, β and γ are constants for calibration. The constant α calibrates the event magnitude, and constants β and γ calibrate the influences of geometric spreading and anelastic absorption (Bakun 2006; Pasolini et al. 2008). The constants c, α, β and γ are determined using a least-squares fitting so as to minimize the mean squared errors between the instrumental seismic intensities and the theoretical seismic intensity attenuation curve.

The mean-squared error (MSE), ϕ, is defined to be

$$\phi(c, \alpha, \beta, \gamma) = \sum_{j=1}^{N_e} \sum_{i=1}^{N_d} \times \left[n_{ij} \left\{ \overline{I_{ij}^{\mathrm{ins}}} - \left(c + \alpha M_j - \beta \ln(R_i) - \gamma R_i \right) \right\}^2 \right], \qquad (5)$$

where Ne is the number of earthquakes, Nd is the number of discrete distance bins, $\overline{I_{ij}^{\text{ins}}}$ is the average instrumental seismic intensity in hypocentral distance R_i from event j, M_j is the magnitude of event j, and n_{ij} is the weighting factor accounting for the number of data points in the hypocentral distance bin i for event j. When the constants are assumed to be independent variables, those yielding the minimum MSE satisfy $\frac{\partial\phi}{\partial c} = \frac{\partial\phi}{\partial\alpha} = \frac{\partial\phi}{\partial\beta} = \frac{\partial\phi}{\partial\gamma} = 0$ (Cheney and Kincaid 2007). The constants can be determined by solving a linear equation system.

4.3. *Seismic-Intensity Anomalies*

The seismic-intensity anomaly, ΔI_i, is calculated from the stacked residuals between the observed and expected seismic intensities

$$\Delta I_i = \frac{1}{N_i}\sum_{j=1}^{N_i}\left(I_{ij}^{\text{ins}} - I_{ij}^{\text{exp}}\right), \qquad (6)$$

where N_i is the number of events recorded at location i, I_{ij}^{ins} is the instrumental seismic intensity at location i for event j, and I_{ij}^{exp} is the expected seismic intensity calculated according to Eq. (4).

The study area is discretized by uniform bins. The stacked seismic-intensity anomaly at spatial bin j, $\overline{\Delta I_j}$, is given by

$$\overline{\Delta I_j} = \frac{1}{Z_j}\sum_{i=1}^{Z_j}\Delta I_i|_j, \qquad (7)$$

where $\Delta I_i|_j$ is the seismic intensity anomaly at location i that belongs to spatial bin j, and Z_j is the number of observed seismic-intensity anomalies in spatial bin j.

5. *Estimation of Seismic Intensities*

A limited number of people-felt macroseismic intensities are available in a stable region. Instrumental seismic intensities are complemented to expand the seismic intensity data set, which is expected to enhance the stability and accuracy of analyses. Conventional seismic intensity scales are based on an ordinary numbering system in which the levels are assigned positive integers. In this study, we determine the instrumental seismic intensities in rational number to reduce the effect of roundoff errors in the calculation of seismic intensity anomalies.

The instrumental seismic intensities are calculated with the seismic wavetrains from the first-arrival P (Pg or Pn) to the Rg coda (Fig. 3c). For practical application, waveforms in traveltimes between $l/6.05 - 4.2$ and $l/2 + 50$ s are analyzed for events within epicentral distances l less than 106 km, and between $l/7.95$ and $l/2 + 50$ s for events in epicentral distances greater than 106 km (Hong 2013). Seismic waveforms with signal-to-noise ratios greater than 2 are analyzed. The level of ambient seismic noises is calculated from the 5-s-long wavetrains before the first-arrival P waves.

The seismic-wave attenuation is frequency-dependent, and the frequency content of ground motion changes with distance (e.g., Gutenberg 1958; Attewell and Ramana 1966; Anderson et al. 1977; Boore 1983). This feature suggests that proper determination of the frequency band is important for calculation of seismic intensities. The frequency band (f_1, f_2) is adjusted to minimize the errors between the reported macroseismic intensities (I^{rep}) and calculated instrumental seismic intensities (I^{ins}). The optimal frequency band is searched from 0.5 to 15.0 Hz.

The constants k_1 and k_2 are determined for each frequency band using least-squares fitting of $\bar{S}$ for every MMI scale (Fig. 4). We generally observe large errors between the reported macroseismic intensities and the calculated instrumental seismic intensities at low and high frequencies. We find the minimum errors around 7 Hz for events of all distances and magnitudes. We thus design the optimal frequency band to be 4–10 Hz which has the central frequency to be 7 Hz. The instrumental seismic intensity scaling for the optimal frequency band is determined by (Fig. 5a)

$$I = 3.11(\pm 0.13)\log\bar{S} + 10.61(\pm 0.08). \qquad (8)$$

The mean difference between the reported macroseismic intensities and the estimated instrumental seismic intensities is close to zero (6×10^{-4} in MMI units), and the standard deviation is 1.44 in MMI units. The observation suggests that the instrumental

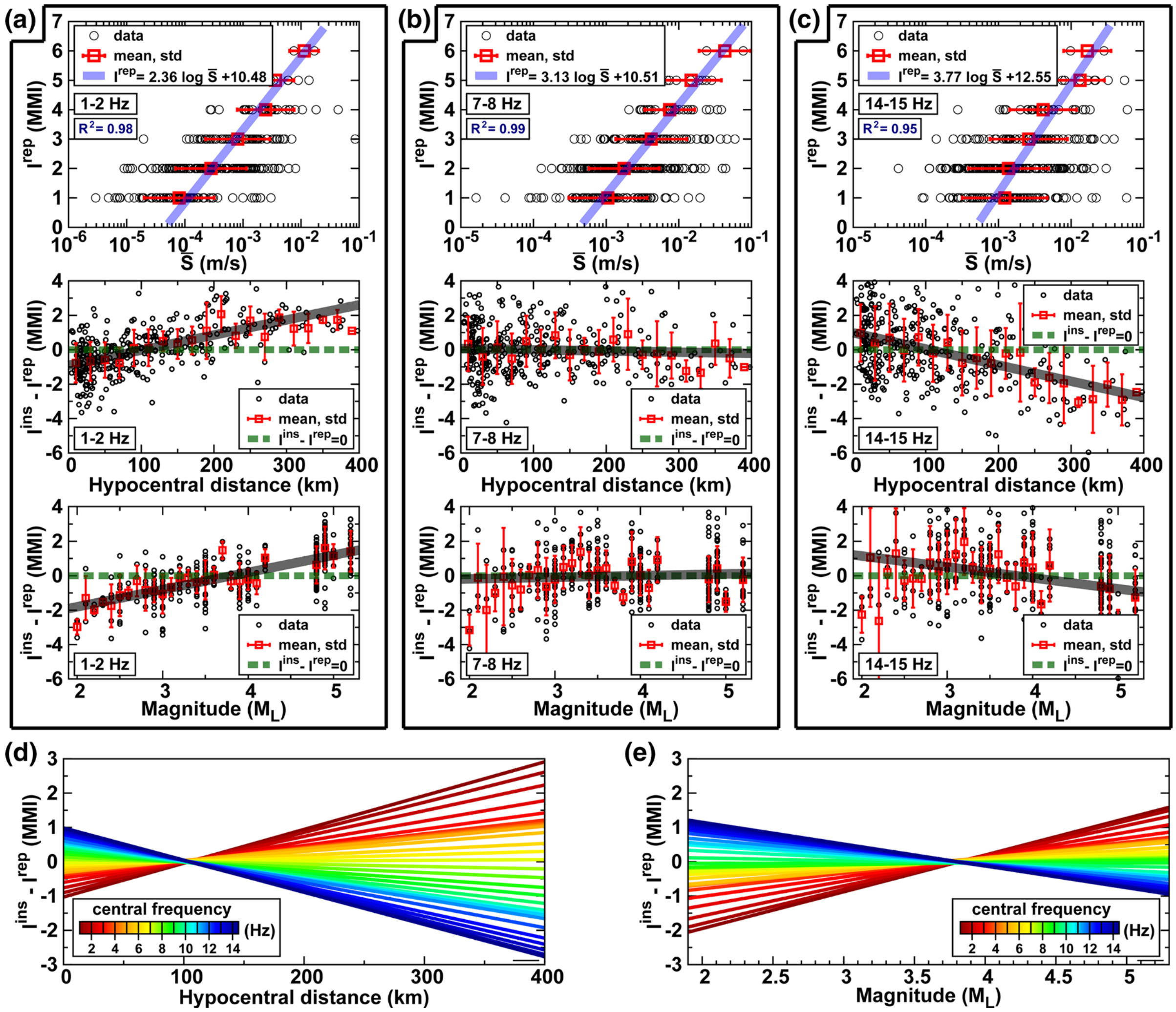

Figure 4

Determination of seismic intensity scales for frequency bands of **a** 1–2 Hz, **b** 7–8 Hz, and **c** 14–15 Hz. (*Top*) derivation of seismic intensity (I) scale as a function of the the log-average spectral amplitude of ground acceleration ($\bar{S}$). The means and standard deviations of $\bar{S}$ for every MMI levels are presented with *squares* and *bars*. The least-squares-fitted lines (*solid lines*) to the mean values are presented with the correlation coefficients (R^2). Distribution of differences between the estimated instrumental seismic intensities and the reported macroseismic intensities ($I^{ins} - I^{rep}$) as a function of distance (*middle*) and magnitude (*bottom*). The means and standard deviations of the differences in every distance and magnitude bins are marked. The linear least-squares fitting lines are presented with *solid lines*. The best-fitting lines match well with the means of data points. Variations in differences between the instrumental seismic intensities and the reported macroseismic intensities ($I^{ins} - I^{rep}$) as a function of **d** distance, and **e** magnitude for changes of frequency bands are presented. The mean errors are around zero for frequencies around 7 Hz

seismic intensity scale represents the macroseismic intensity reasonably (Fig. 5b). The instrumental seismic intensity scale is applicable for events with magnitudes greater than 2.2 at distances up to 400 km (Fig. 5c, d).

In Fig. 6, we present examples of the calculated instrumental seismic intensities for moderately-sized events, which are the 26 April 2004 M_L 3.9 earthquake, the 20 Jan 2007 M_L 4.8 earthquake, and the 1 May 2009 M_L 4.0 earthquake. The seismic intensities display local variations among adjacent locations, suggesting the dominant influence of subsurface structure upon seismic intensities. In addition, the seismic intensities present characteristic regional

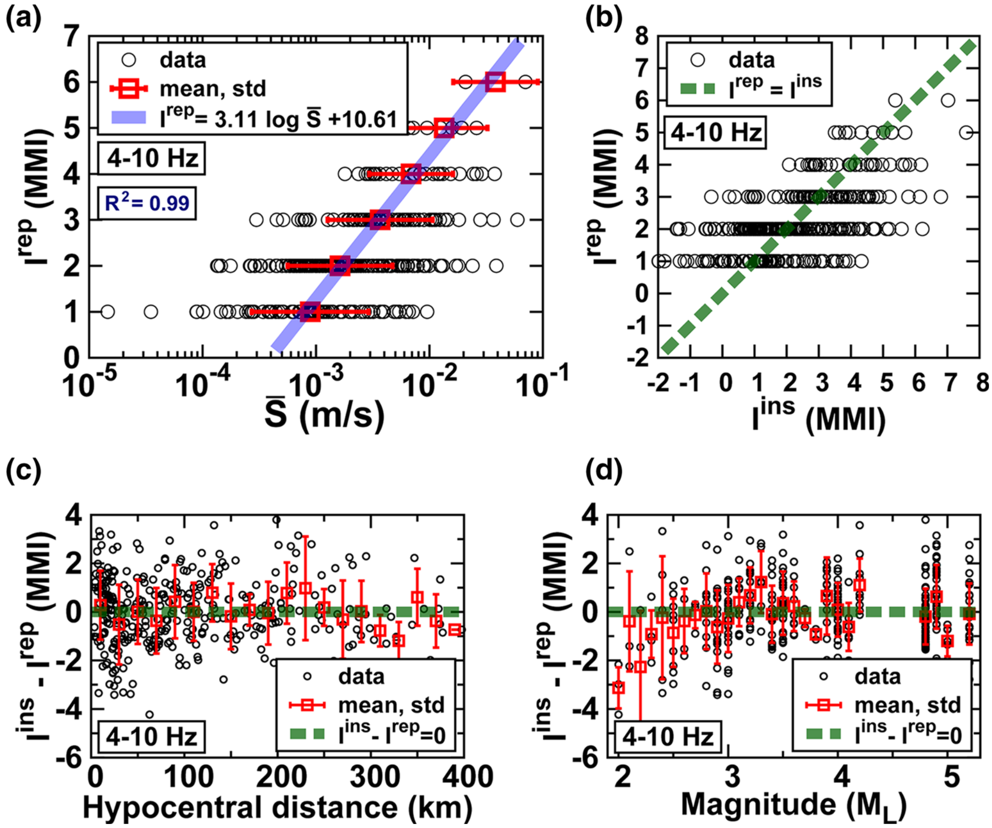

Figure 5

a Variation in instrumental seismic intensities (I^{ins}) as a function of the log-average spectral amplitude of ground acceleration ($\bar{S}$) for the representative frequency band (4–10 Hz). The means and standard deviations of the estimated seismic intensities are marked with *squares* and *bars*. The relationship between I^{rep} and $\bar{S}$ is presented with a *solid line*. The correlation coefficients (R^2) are marked. **b** Comparison between the reported macroseismic intensities (I^{rep}) and the estimated instrumental seismic intensities (I^{ins}). The mean error ($I^{\text{ins}} - I^{\text{rep}}$) is 6×10^{-4} in MMI units, and the standard error is 1.44 in MMI units. **c** Differences between the estimated instrumental seismic intensities and the reported macroseismic intensities ($I^{\text{ins}} - I^{\text{rep}}$) as a function of hypocentral distance. The means and standard deviations are marked with *squares* and *bars*. The differences are clustered around zero. **d** Variation in ($I^{\text{ins}} - I^{\text{rep}}$) as a function of magnitude. The means are close to zero for magnitudes greater than 2.2

anomalies (e.g., the central Okcheon belt region for the 26 April 2004 M_{L} 3.9 earthquake, the central Yeongnam massif region for the 20 Jan 2007 M_{L} 4.8 earthquake, and the northeastern Yeongnam massif region for the 1 May 2009 M_{L}4.0 earthquake).

The observed seismic intensities generally decay with distance. The distance-dependent attenuation rates are generally consistent between the reported macroseismic intensities and instrumental seismic intensities (Figs. 3b, 6). In addition, the average strengths of instrumental seismic intensities agree with the reported macroseismic intensities in most regions except some localized areas (e.g., the central Okcheon belt region) (Fig. 6). This localized disagreement may be caused by inhomogeneous spatial coverage of the reported macroseismic intensities and roundoff errors in macroseismic intensities.

6. *Seismic Intensity Decay with Distance*

We determine the instrumental seismic intensities for events with magnitudes greater than 2.2 in distances less than 400 km. The equation of instrumental seismic intensity attenuation as a function of distance is determined. The instrumental seismic intensities between 0.5 and 6.5 are analyzed considering the range of the collected macroseismic intensities. The constants in Eq. (4) are determined to be $c = -0.998$, $\alpha = 1.72$, $\beta = 0.643$, and $\gamma = 0.00608$ (Fig. 6).

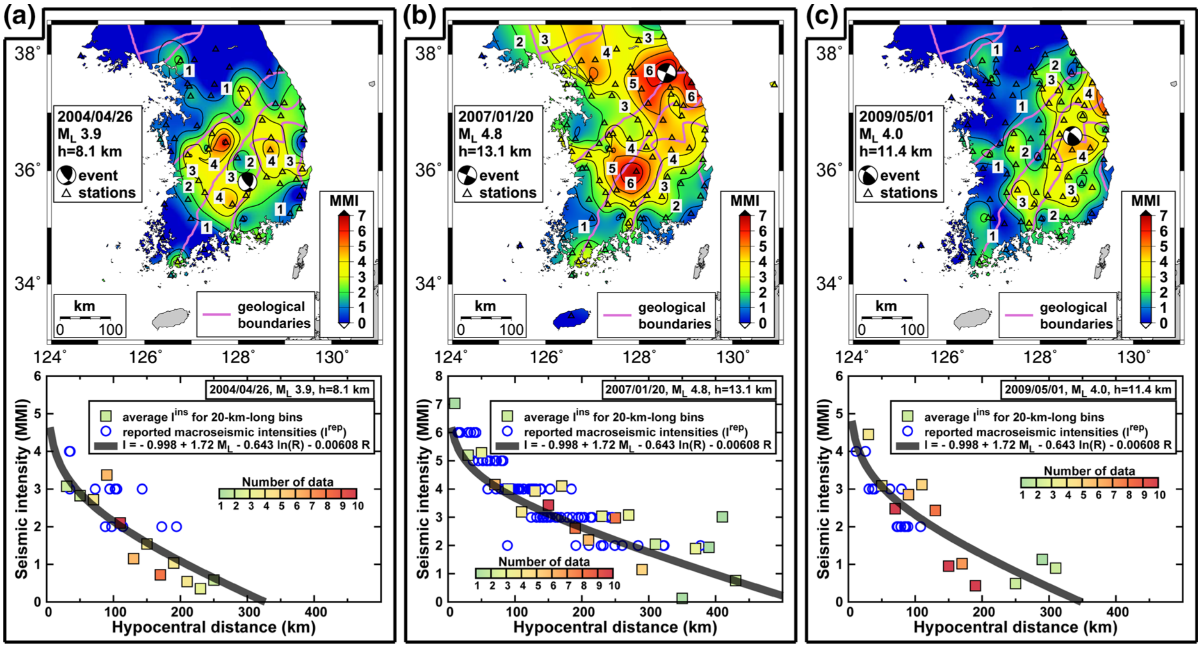

Figure 6

Spatial distribution of instrumental seismic intensities and distance-dependent decrease of seismic intensities: **a** the 26 April 2004 M_L 3.9 earthquake, **b** the 20 Jan 2007 M_L 4.8 earthquake, and **c** the 1 May 2009 M_L 4.0 earthquake. The focal depths (*h*) are 8.1, 13.1, and 11.4 km, respectively. The focal mechanism solutions of events are presented on the maps (Lee and Baag 2008; Kim and Park 2010; Kim et al. 2010; Choi and Noh 2010; Hong and Choi 2012). Geological structures and equi-seismic-intensity contours are marked on the maps. The locations of stations at which instrumental seismic intensities are measured are denoted by triangles on the maps. The reported macroseismic intensities (I^{rep}, *open circles*) and average instrumental seismic intensities of every 20-km distance range (I^{ins}, *filled squares*) are compared in the distance-dependent seismic intensity diagrams. The number of data in each 20-km-long bin is presented. The instrumental seismic intensities agree well with the reported macroseismic intensities. The regression curves for the seismic intensities based on Eq. 8) are presented (*solid line*)

The stability of the inverted parameters is tested using a bootstrap analysis (Efron and Tibshirani 1986). We prepare 1000 bootstrap data sets that are randomly sampled with allowance for selection of data points multiple times from the original data set. The parameters are determined for each bootstrap data set. The means and standard errors of the inverted parameters are estimated (Fig. 7). The standard errors of the inverted parameters from the bootstrap data sets are 0.371 for c, 0.0694 for α, 0.0927 for β, and 0.000795 for γ.

Here, we examine the normality in the distribution of inverted parameters using the χ^2 test that measures the fitness of observed data distribution to a reference normal distribution (Bendat and Piersol 2010). The p value from the χ^2 test varies ranges between 0 and 1. A data set is generally regarded to follow a normal distribution when p value is greater than 0.05. We find the p values to be 0.10 for c, 0.36 for α, 0.59 for β, and 0.91 for γ. The test suggests that the distribution of the inverted parameters generally follow normal distributions (Fig. 7).

The seismic intensity attenuation equation is given by

$$I(M_L, l, h) = -0.998(\pm 0.222) + 1.72(\pm 0.04)M_L - 0.322(\pm 0.027)\ln(\mathrm{l}^2 + \mathrm{h}^2) - 0.00608(\pm 0.00049)\sqrt{l^2 + h^2}, \tag{9}$$

where ML is the local magnitude, and l and h are in km. The average difference between the reported macroseismic intensities and the seismic intensity attenuation curve is determined to be 0.0251 in MMI units, and the standard deviation is 0.649 in MMI units. The 95 % differences ranges between −1.30 and 1.30 in MMI units. From Eq. (9), the seismic intensity may decrease by 1, 2, and 3 MMI unit at an epicentral distance of 35, 97, and 190 km when the focal depth is 10 km (Fig. 8). Also, the seismic

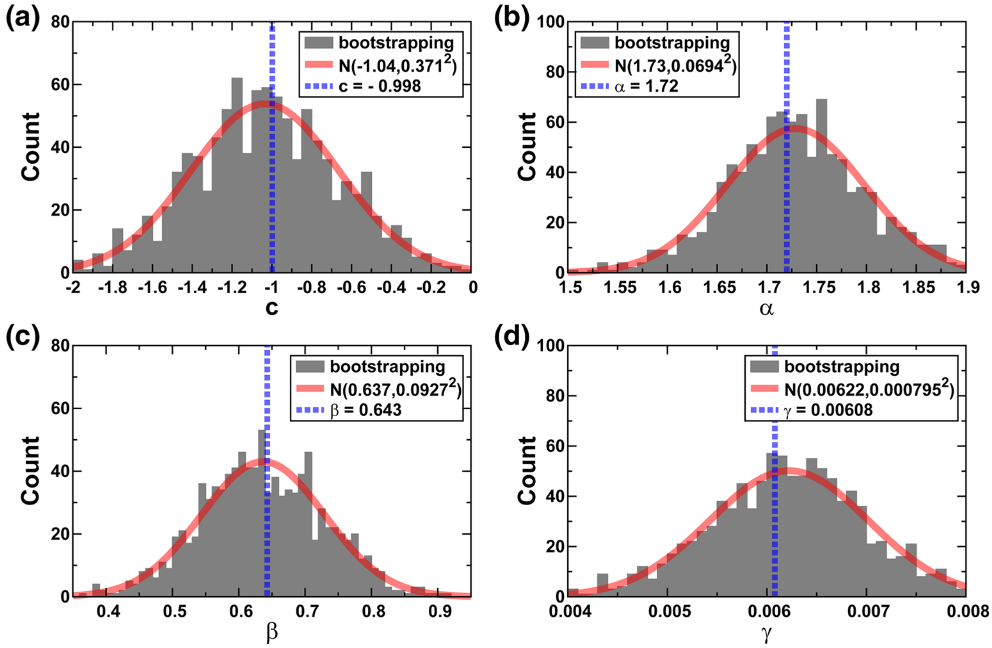

Figure 7
Variation of inverted constants **a** c, **b** α, **c** β, and **d** γ in a bootstrap analysis with 1000 data sets. The inverted constants display normal distributions (*solid line*). The averages and standard errors are presented

intensities may be greater than MMI 5 when an event with magnitude of M_L 7.0 occurs at a distance less than 370 km.

The seismic intensity attenuation curve of this study is generally consistent with those for stable regions including western Australia (Gaull et al. 1990), the United Kingdom (Musson 2005), central Europe (Stromeyer and Grünthal 2009), Indian craton (Szeliga et al. 2010), and eastern North America (Bakun et al. 2011) (Table 1; Fig. 8). It is noteworthy that the seismic intensity attenuation curves for stable regions are separated well from those for active tectonic regions such as New Zealand (Dowrick 1991), the Balkan peninsula (Papazachos and Papaioannou 1997), northern Algeria (Boughacha et al. 2004), western North America (Bakun 2006), northwestern Turkey (Sørensen et al. 2009), Ecuador (Beauval et al. 2010), and the Himalayas (Szeliga et al. 2010). Here note that various seismic intensity scales inclduing the European Macroseismic Scale (EMS-98), Medvedev–Sponheuer–Kárník scale (MSK), and MMI are used in different regions (Table 1). It is known that all the seismic intensity scales are comparable (Sørensen et al. 2009).

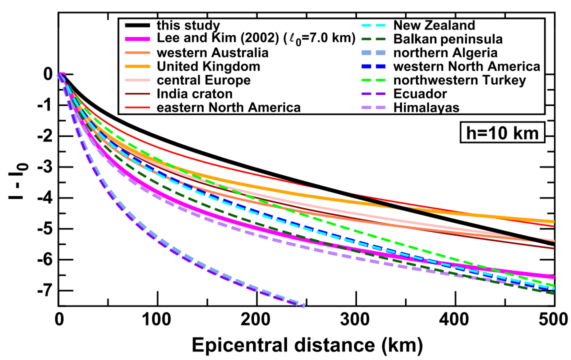

Figure 8
Comparison of the seismic intensity attenuation curves among various regions. The focal depth (h) is set to be 10 km, and I_0 is the epicentral seismic intensity. The seismic intensity attenuation curves for various regions are presented. Stable regions include western Australia (Gaull et al. 1990), the UK (Musson 2005), central Europe (Stromeyer and Grünthal 2009), Indian craton (Szeliga et al. 2010), and eastern North America (Bakun et al. 2011). Active tectonic regions include New Zealand (Dowrick 1991), the Balkan peninsula (Papazachos and Papaioannou 1997), northern Algeria (Boughacha et al. 2004), western North America (Bakun 2006), northwestern Turkey (Sørensen et al. 2009), Ecuador (Beauval et al. 2010), and the Himalayas (Szeliga et al. 2010). A previous study of the Korean Peninsula by Lee and Kim (2002) is also presented for comparison. The seismic intensity attenuation curves are well separated between stable regions and active tectonic regions

Table 1

Seismic intensity attenuation equations of stable and active tectonic regions

Group	Region (reference)	Equation	Data coverage (distance, magnitude)	Scaling
Stable regions	Western Australia (Gaull et al. 1990)	$I = 2.20 + 1.50\,M_L - 1.39\ln(\mathrm{R})$	$R < \sim 900$ km, $4.5 \leq M_L \leq 7.2$	MMI
	Sino-Korean craton (Lee and Kim 2002)	$I - I_0 = 1.75\ln(0.412 + 0.588\,l/l_0)$	$R < \sim 150$ km, $5.0 \leq M \leq 7.5$	MMI
	United Kingdom (Musson 2005)	$I = 3.31 + 1.28\,M_L - 1.22\ln(\mathrm{R})$	$R < \sim 710$ km, $2.0 \leq M_L \leq 6.1$	EMS-98
	Central Europe (Stromeyer and Grünthal 2009)	$I - I_0 = -1.22\ln(R/h) - 0.0013\,(R - h)$	$R < 400$ km, $2.4 \leq M_w \leq 5.7$	EMS-98, MSK
	India craton (Szeliga et al. 2010)	$I = 3.67 + 1.28\,M_w - 1.23\ln(\mathrm{R}) - 0.0017\,\mathrm{R}$	$R < \sim 2000$ km, $4.1 \leq M_w \leq 7.6$	MSK
	Eastern North America (Bakun et al. 2011)	$I = 2.89 + 1.36\,M_w - 0.91\ln(\mathrm{R}) - 0.00277\,\mathrm{R}$	$R < \sim 2000$ km, $3.7 \leq M_w \leq 7.3$	MMI
Active regions	New Zealand (Dowrick 1991)	$I = 2.59 + 1.40\,M - 1.22\ln(\mathrm{R}) - 0.0044\,\mathrm{R}$	$R < 500$ km, $5.0 \leq M \leq 7.8$	MMI
	Balkan peninsula (Papazachos and Papaioannou 1997)	$I - I_0 = -1.40\ln(R/h) - 0.0033\,(R - h)$	$R < 400$ km, $4.1 \leq M_w \leq 7.7$	MMI
	Northern Algeria (Boughacha et al. 2004)	$I - I_0 = -2.26\ln(R/h) - 0.001\,(R - h)$	$R < \sim 280$ km, $3.8 \leq M_b \leq 6.7$	MMI, MSK
	Western North America (Bakun 2006)	$I = 0.44 + 1.70\,M_w - 1.18\ln(\mathrm{R}) - 0.0048\,\mathrm{R}$	$R < 520$ km, $5.5 \leq M_w \leq 7.3$	MMI
	Northwestern Turkey (Sørensen et al. 2009)	$I = 3.42 + 0.793\,M_w - 0.937\ln(\mathrm{R/h}) - 0.0065\,(\mathrm{R - h})$	$R < 350$ km, $5.9 \leq M_w \leq 7.4$	EMS-98, MMI, MSK
	Ecuador (Beauval et al. 2010)	$I = -0.85 + 2.41\,M_w - 2.34\ln(R)$	$R < 76.9$ km, $5.3 \leq M_w \leq 7.1$	MSK
	Himalayas (Szeliga et al. 2010)	$I = 6.05 + 1.11\,M_w - 1.70\ln(R) - 0.0006\,R$	$R < \sim 2700$ km, $4.9 \leq M_w \leq 8.6$	MSK

I_0 epicentral seismic intensity, R hypocentral distance in km, l_0 the radius of region with I_0

The seismic intensities decay fast with distance in active tectonic regions, but slowly in stable regions. This feature is consistent with high seismic attenuation (low Q) in active tectonic regions (Howell and Schultz 1975; Aki 1980; Hwang and Mitchell 1987; Szeliga et al. 2010). This observation suggests that the seismic damage may be concentrated around event epicenters in active tectonic regions. On the other hand, the seismic damage is expected over wider areas in stable regions for events of the same size. Note that the seismic intensity attenuation curve of this study is not consistent with a study on the Korean Peninsula by Lee and Kim (2002), which displays fast attenuation of seismic intensity with distance. This difference may be partly due to the limited data coverage of Lee and Kim (2002), which is based on a few moderately-sized earthquakes.

7. Regional Variation in Seismic Intensities

The seismic intensity anomalies are estimated by stacking the residuals between the instrumental seismic intensities and the reference seismic intensity curves. The stacking of seismic-intensity residuals minimizes the source radiation effects. Stacking residuals over a region presents the regional anomalies in seismic intensities. These seismic intensity anomalies may be associated with relative amplification or diminution of the ground motion in the region.

We analyze the instrumental seismic intensities from 150 stations. The number of instrumental seismic intensities for each station varies from 1 to 29. The seismic intensity anomalies are found to vary between −1.45 and 2.14 in MMI units. The mean and standard deviation of the seismic intensity anomalies

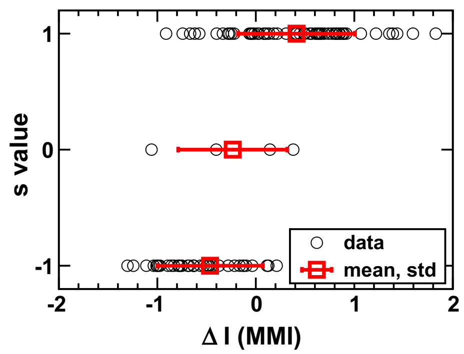

Figure 9
Comparison between the seismic intensity anomalies and the region-dependent ground amplification factor (*s*) of Emolo et al. (2015). The means and standard deviations of seismic intensity anomalies are marked with *squares* and *bars*. A weak correlation between the seismic intensity anomalies and *s* values is observed

are 0.035 and 0.799 in MMI units. The mean value is close to zero, suggesting that the reference seismic intensity attenuation curve well represents the average distance-dependent decay of seismic intensities.

Here, the 0.05 and 0.95 quantiles of the seismic intensity anomalies are −1.11 and 1.44 in MMI units. Also, the 0.25 and 0.75 quantiles are −0.63 and 0.64 in MMI units. The seismic intensity anomalies are expected to vary up to ±1.57 in MMI units with a 95 % confidence level. The seismic intensity anomalies display apparent agreement with the region-dependent ground amplification factor (*s*) of Emolo et al. (2015) (Fig. 9). This observation supports the observed seismic intensity anomalies.

The regional seismic intensity anomalies are assessed by averaging local seismic intensity anomalies in spatial bins with a size of 0.8° × 0.8° at every 0.1° in longitude and latitude. The number of data is more than 10 in most bins (Fig. 10a). The regional seismic intensity anomalies vary between −1.03 and 1.36 in MMI units, and the standard deviation is 0.35 in MMI units (Fig. 10b). The regional seismic intensity anomalies are characteristically correlated with the regional geological and tectonic structures. Positive anomalies are observed in the southern peninsula (the Yeongnam massif and the Gyeongsang basin), while negative anomalies are observed in the central peninsula (the Gyeonggi massif).

The stability of the results is tested using a bootstrap analysis (Efron and Tibshirani 1986; Hong and Menke 2008). The bootstrap test quantifies the influence of each data point in the data set. We prepare 100 bootstrap data sets for each spatial bin. The average results from the bootstrap data sets are close to the results from the original data set (Fig. 11a). The standard errors among the results from the bootstrap data sets are found to be less than 0.20 in regions with the number of data greater than 10 (Fig. 11b). The northeastern marginal region with small numbers of data display relatively high standard errors. This observation confirms the stability of the results, supporting the property of regional-scale variation in seismic intensities.

8. *Comparison with Regional Crustal Properties*

The seismic intensity is generally proportional to the strength of ground motion, which is dependent on the medium properties (e.g., Olsen 2000; Yang and Sato 2000). We compare the regional variations of seismic intensity anomalies with regional crustal properties to infer the influences of regional crustal properties on seismic intensities (Fig. 12).

The seismic intensity anomalies are compared with various crustal properties in every 0.1° longitude and latitude by geological province (Fig. 12). We observe that the data points for all provinces are generally well mixed in the graphs rather than grouped separately. This observation suggest that the correlations between the seismic intensity anomalies and crustal properties are not significantly depending on the geological province. We examine apparent correlations between the seismic intensity anomalies and crustal properties (Fig. 12).

We find positive seismic intensity anomalies in regions with large crustal thickness (Fig. 12a). The crustal thickness controls the Moho topography and lower crustal stress field, which causes seismic amplification or attenuation (e.g., Artyushkov 1973; Frankel 1994). The seismic intensity appears to increase with crustal P amplification (Fig. 12b). We also observe apparent positive correlations between the seismic intensity anomalies and seismicity densities (Fig. 12d). Also, apparent positive correlations were found between the seismic intensity anomalies and shear-wave attenuation (Lg Q_0^{-1}) (Fig. 12c). On

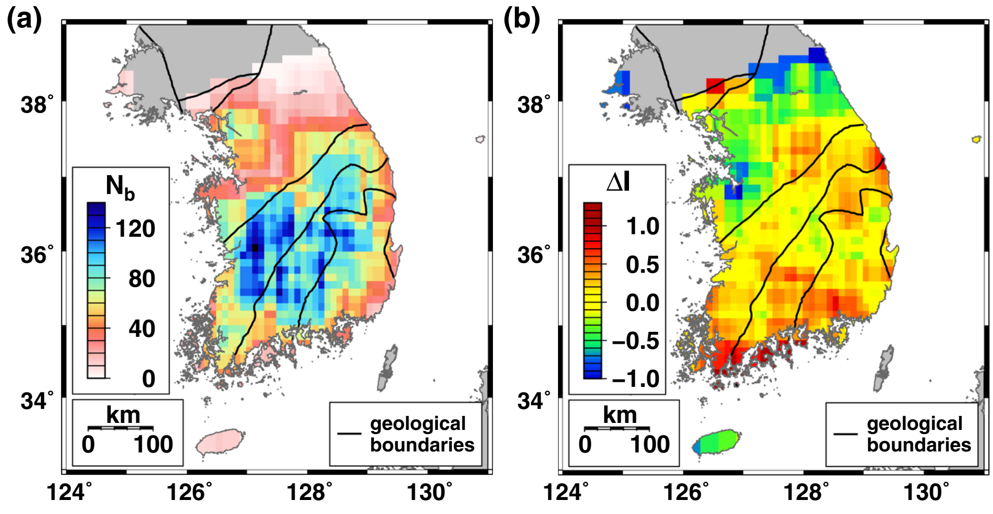

Figure 10

a Numbers of seismic data in spatial bins (*Nb*). The numbers are larger than 10 in most regions of the southern Korean Peninsula. **b** Regional variations in seismic intensity anomalies. Characteristic negative seismic intensity anomalies are observed in the central peninsula around the Gyeonggi massif, while positive anomalies are observed in the southern peninsula around the Yeongnam massif and Gyeongsang basin

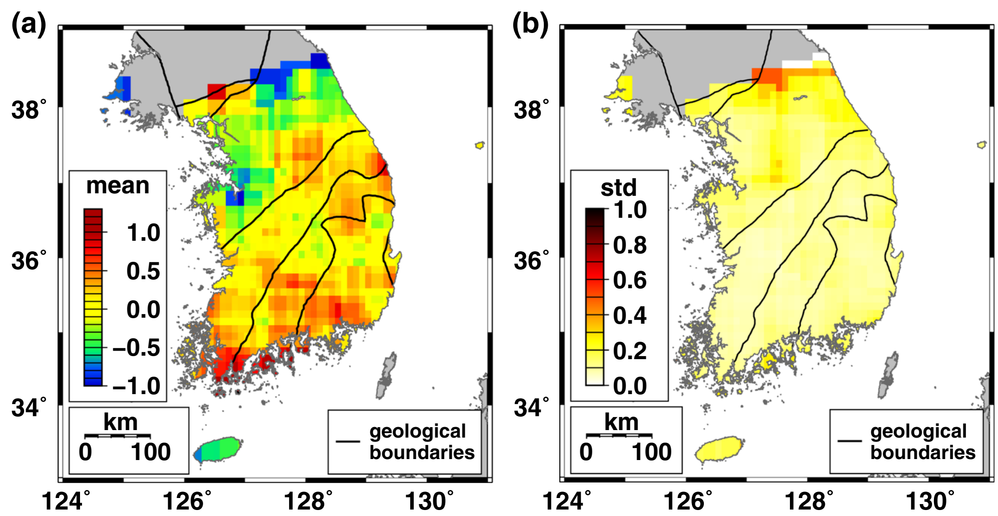

Figure 11

Bootstrap analysis of seismic intensity anomalies. **a** Averages of the results from 100 bootstrap data sets. The averages are close to the results from the original data set. **b** Standard errors among the results from 100 bootstrap data sets. The standard errors are low in most regions except for the marginal region of data coverage

the other hand, the heat flows display anti-correlations with the seismic intensity anomalies (Fig. 12e).

The seismic intensities are high in regions of large crustal thicknesses, large seismicity densities or low heat flows (e.g., Burov 2007). The gravity anomalies may be a composite effect of crustal thickness and thermal components, which produces a mild correlation between seismic intensity anomalies and gravity anomalies (Reilly 1962). We also find exclusively high dependency of the seismic intensity on the presence of a thick sedimentary layer around the Gyeongsang basin where seismic ground motions are amplified strongly by a thick sedimentary layer in the shallow crust (e.g., Bard and Bouchon 1980).

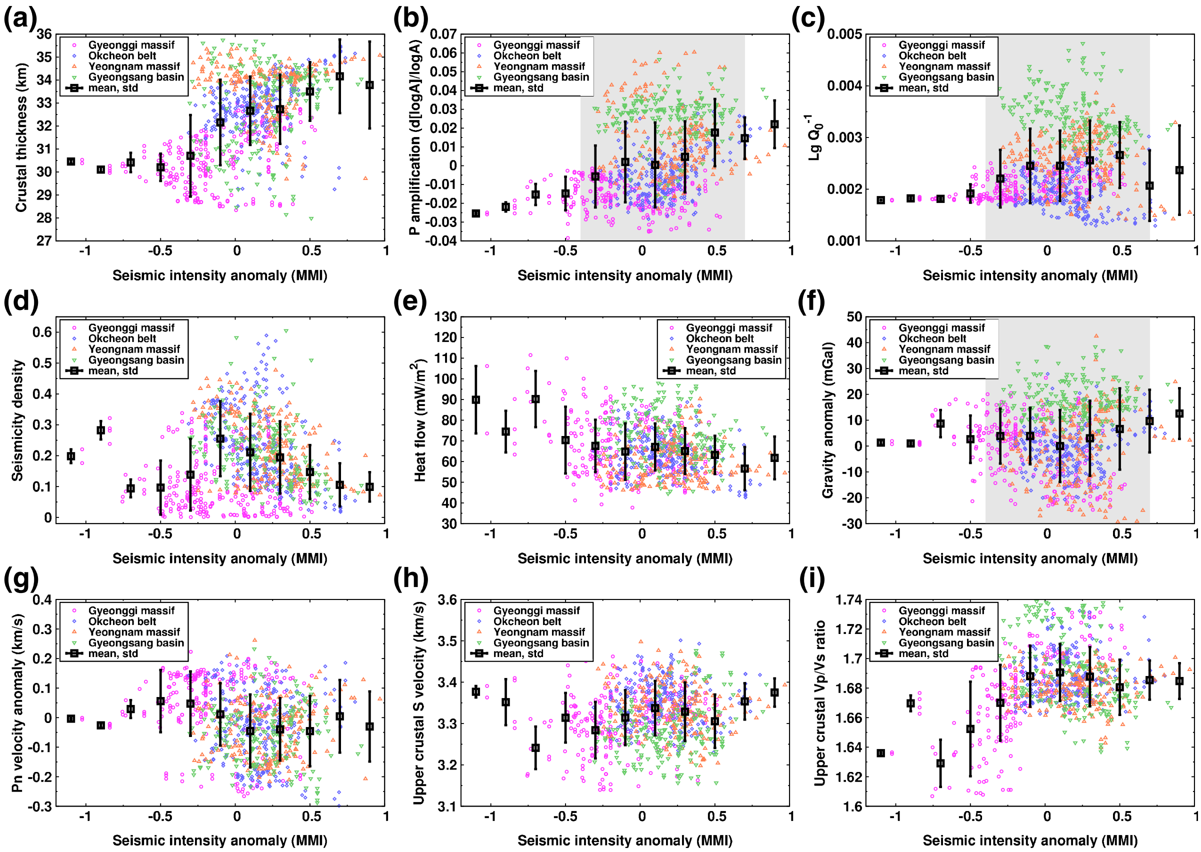

Figure 12
Variation of seismic and geophysical properties of the crust as a function of seismic intensity anomaly: **a** crustal thicknesses, **b** crustal P amplification, **c** crustally-guided shear-wave attenuation (Lg Q_0^{-1}), **d** seismicity densities, C, of earthquakes with magnitudes equal to or larger than 2.5 during 1978–2013, **e** surface heat flows, **f** Bouguer gravity anomalies, **g** variation in Moho P (Pn) velocities relative to 7.95 km s^{-1}, **h** shear-wave velocities at a depth of 6.75 km, and **i** upper-crustal V_P/V_S ratios. The data points are marked by the geological province [Gyeonggi massif (*circles*), Okcheon belt (*diamonds*), Yeongnam massif (*triangles*), and Gyeongsang basin (*inverted triangles*]. The means (*squares*) and standard deviations (*bars*) are presented for every 0.2 MMI bins. The ranges of data points from all geological provinces are *shaded*

However, seismic intensity anomalies display no apparent correlation between seismic intensity anomalies with Bouguer gravity anomalies, Pn velocities, upper-crustal S velocities, and V_P/V_S ratios.

The apparent correlations between the seismic intensities and crustal properties may be related with the modulation of seismic amplitudes and frequency contents depending on the lithological composition, crustal structure, density variation, temperature, heterogeneity, and anelastic effects in the crust. In particular, the medium properties including the density, seismic velocities, and seismic attenuation may be affected by the internal temperatures that are controlled by the heat flows (e.g., Hughes and Maurette 1956; Heard and Page 1982; Fei 1995; Roth et al. 2000). The seismic intensity anomalies are may be a consequence of composite effects of various crustal parameters. Some crustal parameters are interlocked, causing difficulty in distinguishing the sole influence of a certain crustal property.

9. Discussion and Conclusions

We introduced an instrumental seismic intensity scale for the Korean Peninsula. The instrumental seismic intensity scale is calibrated for reported macroseismic intensities. The seismic intensities displayed a characteristic slow decay rate with distance in the Korean Peninsula. The medium properties cause a discriminative amplification and attenuation of seismic waves, producing region-dependent seismic intensity anomalies. The seismic-intensity anomalies between the instrumental seismic intensities and the reference seismic intensity attenuation curve presented local to regional variations.

The amplitudes and spectral contents of seismic waves are highly influenced by the properties of shallow media (e.g., Gao et al. 1996; Semblat et al. 2005; Kanth and Iyengar 2007; Castellaro et al. 2008). We found local variations in the seismic intensities depending on the local subsurface properties.

The regional seismic intensity anomalies were assessed by stacking the local seismic intensity residuals. The regional seismic intensity anomalies presented positive correlations with the P amplifications, and negative correlations with seismic quality factors. The seismic intensity anomalies reached 1.46 in MMI units in the regions of high crustal amplifications (e.g., the south-central Gyeonggi massif, Yeongnam massif, and Okcheon belt). We found high positive seismic intensities in the regions with large crustal thicknesses and low heat flows (e.g., Okcheon belt and Yeongnam massif).

The region of thick sediments (e.g., Gyeongsang basin) produced strong ground motions, increasing regional seismic intensities exclusively (Trifunac and Lee 1989; Konno and Ohmachi 1998; Olsen 2000; Yang and Sato 2000). Also, we find large positive seismic intensity anomalies in the Yeongnam massif and Gyeongsang basin, suggesting high seismic-hazard potentials.

The observations suggest that the seismic intensity anomalies are not only controlled by the local subsurface properties, but also by the regional crustal properties including lithology, crustal structure, thickness, chemical composition, and thermal budget (heat flow). It may be important to consider the crustal properties for better mitigation of potential seismic hazards.

Acknowledgements

We are grateful to Associate Editor Fabio Romanelli and two anonymous reviewers for valuable review comments. This work was supported by the Korea Meteorological Administration Research and Development Program under Grant KMIPA 2015-7040. Also, this research was partly supported by the Basic Science Research Program through the National Research Foundation of Korea (NRF) funded by the Ministry of Education (NRF-2015R1D1A1A01060198).

References

Aki, K. (1980). Scattering and attenuation of shear waves in the lithosphere. *Journal of Geophysical Research*, *85*, 6496–6504.

Anderson, D. L., Kanamori, H., Hart, R. S., & Liu, H.-P. (1977). The earth as a seismic absorption band. *Science*, *196*, 1104–1106.

Ardeleanu, L., Leydecker, G., Bonjer, K. P., Busche, H., Kaiser, D., & Schmitt, T. (2005). Probabilistic seismic hazard map for Romania as a basis for a new building code. *Natural Hazards and Earth System Science*, *5*, 679–684.

Artyushkov, E. V. (1973). Stresses in the lithosphere caused by crustal thickness inhomogeneities. *Journal of Geophysical Research*, *78*, 7675–7708.

Attewell, P. B., & Ramana, Y. V. (1966). Wave attenuation and internal friction as functions of frequency in rocks. *Geophysics*, *31*, 1049–1056.

Bakun, W. H. (2006). MMI attenuation and historical earthquakes in the Basin and Range province of western North America. *Bulletin of the Seismological Society of America*, *96*, 2206–2220.

Bakun, W. H., & Scotti, O. (2006). Regional intensity attenuation models for France and the estimation of magnitude and location of historical earthquakes. *Geophysical Journal International*, *164*, 596–610.

Bakun, W. H., Stickney, M. C., & Rogers, G. C. (2011). The 16 May 1909 Northern Great Plains earthquake. *Bulletin of the Seismological Society of America*, *101*, 3065–3071.

Bard, P. Y., & Bouchon, M. (1980). The seismic response of sediment-filled valleys. Part 1 The case of incident SH waves. *Bulletin of the Seismological Society of America*, *70*, 1263–1286.

Beauval, C., Yepes, H., Bakun, W. H., Egred, J., Alvarado, A., & Singaucho, J.-C. (2010). Locations and magnitudes of historical earthquakes in the Sierra of Ecuador (1587–1996). *Geophysical Journal International*, *181*, 1613–1633.

Bendat, J. S., & Piersol, A. G. (2010). Statistical principles. *Random data: Analysis and measurement procedures* (4th ed.). Hoboken: Wiley. doi:10.1002/9781118032428.ch4.

Boore, D. M. (1983). Stochastic simulation of high-frequency ground motions based on seismological models of the radiated spectra. *Bulletin of the Seismological Society of America*, *73*, 1865–1894.

Borcherdt, R. D., & Gibbs, J. F. (1976). Effects of local geological conditions in the San Francisco Bay region on ground motions and the intensities of the 1906 earthquake. *Bulletin of the Seismological Society of America*, *66*, 467–500.

Boughacha, M. S., Ouyed, M., Ayadi, A., & Benhallou, H. (2004). Seismicity and seismic hazard mapping of northern Algeria: Map of maximum calculated intensities (MCI). *Journal of Seismology*, *8*, 1–10.

Burov, E. B. (2007). Plate rheology and mechanics. In A. B. Watts (Ed.), *Crust and lithosphere dynamics, treatise on geophysics* (Vol. 6, pp. 100–151). Oxford: Elsevier.

Casado, C. L., Palacios, S. M., Delgado, J., & Peláez, J. A. (2000). Attenuation of intensity with epicentral distance in the Iberian Peninsula. *Bulletin of the Seismological Society of America*, *90*, 34–47.

Castellaro, S., Mulargia, F., & Rossi, P. L. (2008). VS30: Proxy for seismic amplification? *Seismological Research Letters*, *79*, 540–543.

Chandler, A. M., & Lam, N. T. (2002). Intensity attenuation relationship for the South China region and comparison with the component attenuation model. *Journal of Asian Earth Sciences*, *20*, 775–790.

Chang, E. Z. (1996). Collisional orogene between north and south China and its eastern extension in the Korean Peninsula. *Journal of Southeast Asian Earth Sciences*, *13*, 267–277.

Chang, S. J., & Baag, C.-E. (2007). Moho depth and crustal V_P/V_S variation in southern Korea from teleseismic receiver functions: Implication for tectonic affinity between the Korean peninsula and China. *Bulletin of the Seismological Society of America*, *97*, 1621–1631.

Cheney, W., & Kincaid, D. (2007). *Numerical Mathematics and Computing*. Pacific Grove: Brooks/Cole Publishing company.

Cho, J.-D., Choi, J.-H., Lim, M.-T., Park, I.-H., & Ko, I.-S. (1997). A Study on the regional gravity anomaly (Southern Part of Korean Peninsula), KIGAM Research Report KR-96 (c)-5, Korea Institute of Geology and Mining and Materials, pp. 27 **(in Korean)**.

Choi, H., & Noh, M. (2010). Source parameters of the May 2, 2009 Andong earthquake in South Korea. *Geosciences Journal*, *14*, 269–276.

Choi, J., Kang, T.-S., & Baag, C.-E. (2009). Three-dimensional surface wave tomography for the upper crustal velocity structure of southern Korea using seismic noise correlations. *Geosciences Journal*, *13*, 423–432.

Chough, S. K., & Barg, E. (1987). Tectonic history of Ulleung basin margin, East Sea (Sea of Japan). *Geology*, *15*, 45–48.

Chough, S. K., Kwon, S. T., Ree, J. H., & Choi, D. K. (2000). Tectonic and sedimentary evolution of the Korean peninsula: A review and new view. *Earth Science Reviews*, *52*, 175–235.

Cornell, C. A. (1968). Engineering seismic risk analysis. *Bulletin of the Seismological Society of America*, *58*, 1583–1606.

Davenport, P. N. (2001). Seismic intensities derived from strong motion instruments in New Zealand. In: Proceedings of the Technical Conference of the New Zealand Society for Earthquake Engineering (NZSEE 2001), Wairakei, New Zealand, 2001, Paper No. 4.03.01.

DeMets, C., Gordon, R. G., & Argus, D. F. (2010). Geologically current plate motions. *Geophysical Journal International*, *181*, 1–80.

Dowrick, D. J. (1991). A revision of attenuation relationships for Modified Mercalli intensity in New Zealand earthquakes. *Bulletin of the New Zealand National Society for Earthquake Engineering*, *24*, 210–224.

Efron, B., & Tibshirani, R. (1986). Bootstrap methods for standard errors, confidence intervals, and other measures of statistical accuracy. *Statistical Science*, *1*, 54–75.

Emolo, A., Sharma, N., Festa, G., Zollo, A., Convertito, V., Park, J.-H., et al. (2015). Ground-Motion Prediction Equations for South Korea Peninsula. *Bulletin of the Seismological Society of America*, *105*, 2625–2640.

Fei, Y. (1995). Thermal expansion. In T. J. Ahrens (Ed.), *Mineral physics and crystallography: A handbook of physical constants* (Vol. 2, pp. 29–44). Washington, DC: American Geophysical Union.

Frankel, A. (1994). Dense array recordings in the San Bernardino Valley of Landers-Big Bear aftershocks: Basin surface waves, Moho reflections, and three-dimensional simulations, *Bulletin of the Seismological Society of America*, *84*, 613–624.

Gao, S., Liu, H., Davis, P. M., & Knopoff, L. (1996). Localized amplification of seismic waves and correlation with damage due to the Northridge earthquake: evidence for focusing in Santa Monica. *Bulletin of the Seismological Society of America*, *86*, S209–S230.

Gasperini, P., Bernardini, F., Valensise, G., & Boschi, E. (1999). Defining seismogenic sources from historical earthquake felt reports. *Bulletin of the Seismological Society of America*, *89*, 94–110.

Gaull, B. A., Michael-Leiba, M. O., & Rynn, J. M. W. (1990). Probabilistic earthquake risk maps of Australia. *Australian Journal of Earth Sciences*, *37*, 169–187.

Geli, L., Bard, P. Y., & Jullien, B. (1988). The effect of topography on earthquake ground motion: A review and new results. *Bulletin of the Seismological Society of America*, *78*, 42–63.

Gupta, I. N., & Nuttli, O. W. (1976). Spatial attenuation of intensities for central US earthquakes. *Bulletin of the Seismological Society of America*, *66*, 743–751.

Gutenberg, B. (1958). Attenuation of seismic waves in the earth's mantle. *Bulletin of the Seismological Society of America*, *48*, 269–282.

Hancock, J., & Bommer, J. J. (2006). A state-of-knowledge review of the influence of strong-motion duration on structural damage. *Earthquake Spectra*, *22*, 827–845.

Hanks, T. C., & McGuire, R. K. (1981). The character of high-frequency strong ground motion. *Bulletin of the Seismological Society of America*, *71*, 2071–2095.

Heard, H. C., & Page, L. (1982). Elastic moduli, thermal expansion, and inferred permeability of two granites to 350 C and 55 megapascals. *Journal of Geophysical Research*, *87*, 9340–4348.

Helffrich, G. R., & Wood, B. J. (2001). The Earth's mantle. *Nature*, *412*, 501–507.

Heki, K., Miyazaki, S. I., Takahashi, H., Kasahara, M., Kimata, F., Miura, S., et al. (1999). The Amurian Plate motion and current plate kinematics in eastern Asia. *Journal of Geophysical Research*, *104*, 29147–29155.

Hinzen, K.-G., & Oemisch, M. (2001). Location and magnitude from seismic intensity data of recent and historic earthquakes in the Northern Rhine Area, Central Europe. *Bulletin of the Seismological Society of America*, *91*, 40–56.

Hirata, N., Tokuyama, H., & Chung, T. W. (1989). An anomalously thick layering of the crust of the Yamato Basin, southeastern Sea of Japan: The final stage of back-arc spreading. *Tectonophysics*, *165*, 303–314.

Hong, T.-K. (2010). *Lg* attenuation in a region with both continental and oceanic environments. *Bulletin of the Seismological Society of America*, *100*, 851–858.

Hong, T.-K. (2013). Seismic discrimination of the 2009 North Korean nuclear explosion based on regional source spectra. *Journal of Seismology*, *17*, 753–769.

Hong, T.-K., & Choi, H. (2012). Seismological constraints on the collision belt between the North and South China blocks in the Yellow Sea. *Tectonophysics*, *570*, 102–113.

Hong, T.-K., & Kang, T.-S. (2009). Pn travel-time tomography of the paleo-continental-collision and rifting zone around Korea and Japan. *Bulletin of the Seismological Society of America*, *99*, 416–421.

Hong, T.-K., & Kennett, B. L. N. (2002). On a wavelet-based method for the numerical simulation of wave propagation. *Journal of Computational Physics*, *183*, 577–622.

Hong, T.-K., & Lee, K. (2012). $m_b(Pn)$ Scale for the Korean Peninsula and site-dependent *Pn* amplification. *Pure and Applied Geophysics*, *169*, 1963–1975.

Hong, T.-K., & Menke, W. (2008). Imaging laterally varying regional heterogeneities from seismic coda using a source-array analysis. *Physics of the Earth and Planetary Interiors*, *166*, 188–202.

Hong, T.-K., Lee, J., & Houng, S. E. (2015). Long-term evolution of intraplate seismicity in stress shadows after a megathrust. *Physics of the Earth and Planetary Interiors*, *245*, 59–70.

Hong, T.-K., Park, S., & Houng, S. E. (2016). Seismotectonic properties and zonation of the far-eastern Eurasian plate around the Korean Peninsula. *Pure and Applied Geophysics*, *173*, 1175–1195.

Hong, T.-K., Baag, C.-E., Choi, H., & Sheen, D.-H. (2008). Regional seismic observations of the 9 October 2006 underground nuclear explosion in North Korea and the influence of crustal structure on regional phases. *Journal of Geophysical Research*, *113*, B03305. doi:10.1029/2007JB004950.

Houng, S. E., & Hong, T.-K. (2013). Probabilistic analysis of the Korean historical earthquake records. *Bulletin of the Seismological Society of America*, *103*, 2782–2796.

Howell, B. F., & Schultz, T. R. (1975). Attenuation of modified Mercalli intensity with distance from the epicenter. *Bulletin of the Seismological Society of America*, *65*, 651–665.

Hughes, D. S., & Maurette, C. (1956). Variation of elastic wave velocities in granites with pressure and temperature. *Geophysics*, *21*, 277–284.

Hwang, H. J., & Mitchell, B. J. (1987). Shear velocities, Q_β, and the frequency dependence of Q_β in stable and tectonically active regions from surface wave observations. *Geophysical Journal International*, *90*, 575–613.

Jin, A., & Aki, K. (1989). Spatial and temporal correlation between coda Q^{-1} and seismicity and its physical mechanism. *Journal of Geophysical Research*, *94*, 14041–14059.

Jo, E., & Hong, T.-K. (2013). V_P/V_S ratios in the upper crust of the southern Korean Peninsula and their correlations with seismic and geophysical properties. *Journal of Asian Earth Sciences*, *66*, 204–214.

Kanth, S. R., & Iyengar, R. N. (2007). Estimation of seismic spectral acceleration in peninsular India. *Journal of Earth System Science*, *116*, 199–214.

Kawase, H., & Aki, K. (1990). Topography effect at the critical SV-wave incidence: Possible explanation of damage pattern by the Whittier Narrows, California, earthquake of 1 October 1987. *Bulletin of the Seismological Society of America*, *80*, 1–22.

Kim, H. J., Jou, H.-T., Cho, H.-M., Bijwaard, H., Sato, T., Hong, J.-K., et al. (2003). Crustal structure of the continental margin of Korea in the East Sea (Japan Sea) from deep seismic sounding data: evidence for rifting affected by the hotter than normal mantle. *Tectonophysics*, *364*, 25–42.

Kim, K.-H., & Park, Y. (2010). The 20 January 2007 M_L 4.8 Odaesan earthquake and its implications for regional tectonics in Korea. *Bulletin of the Seismological Society of America*, *100*, 1395–1405.

Kim, W.-Y., Choi, H., & Noh, M. (2010). The 20 January 2007 Odaesan, Korea, earthquake sequence: Reactivation of a buried strike-slip fault? *Bulletin of the Seismological Society of America*, *100*, 1120–1137.

Konno, K., & Ohmachi, T. (1998). Ground-motion characteristics estimated from spectral ratio between horizontal and vertical components of microtremor. *Bulletin of the Seismological Society of America*, *88*, 228–241.

Korea Meteorological Administration. (2002) *Seismological Annual Report 2001*, Dongjin, Seoul, 5–10 **(in Korean)**.

Korea Meteorological Administration. (2003). *Seismological Annual Report 2002*, Dongjin, Seoul, 6–14 **(in Korean)**.

Korea Meteorological Administration. (2004). *Seismological Annual Report 2003*, Dongjin, Seoul, 6–17 **(in Korean)**.

Korea Meteorological Administration. (2005). *Seismological Annual Report 2004*, Dongjin, Seoul, 55–64 **(in Korean)**.

Korea Meteorological Administration. (2006). *Seismological Annual Report 2005*, Dongjin, Seoul, 4–104 **(in Korean)**.

Korea Meteorological Administration. (2007). *Seismological Annual Report 2006*, Dongjin, Seoul, 4–131 **(in Korean)**.

Korea Meteorological Administration. (2008). *Seismological Annual Report 2007*, Dongjin, Seoul, 4–73 **(in Korean)**.

Korea Meteorological Administration. (2009). *Seismological Annual Report 2008*, Dongjin, Seoul, 4–81 **(in Korean)**.

Korea Meteorological Administration. (2010). *Seismological Annual Report 2009*, Dongjin, Seoul, 4–109 **(in Korean)**.

Korea Meteorological Administration. (2011). *Seismological Annual Report 2010*, Dongjin, Seoul, 4–73 **(in Korean)**.

Korea Meteorological Administration. (2012). *Seismological Annual Report 2011*, Dongjin, Seoul, 4–111 **(in Korean)**.

Korea Meteorological Administration. (2013). *Seismological Annual Report 2012*, Dongjin, Seoul, 4–119 **(in Korean)**.

Korea Meteorological Administration. (2014). *Seismological Annual Report 2013*, Dongjin, Seoul, 4–195 **(in Korean)**.

Kyung, J. B., Huh, S. Y., Do, J. Y., & Cho, D. (2007). Relation of intensity, fault plane solutions and fault of the January 20, 2007 Odaesan earthquake ($M_L = 4.8$). *Journal of Korean Earth Science Society*, *28*, 202–213. (in Korean).

Lee, W., & Baag, C.-E. (2008). Local crustal structures of southern Korea from joint analysis of waveforms and travel times. *Geosciences Journal*, *12*, 419–428.

Lee, Y., Park, S., Kim, J., Kim, H. C., & Koo, M. H. (2010). Geothermal resource assessment in Korea. *Renewable and Sustainable Energy Reviews*, *14*, 2392–2400.

Lee, K., & Kim, J.-K. (2002). Intensity attenuation in the Sino-Korean craton. *Bulletin of the Seismological Society of America*, *92*, 783–793.

Main, I. G., Peacock, S., & Meredith, P. G. (1990). Scattering attenuation and the fractal geometry of fracture systems. *Pure and Applied Geophysics*, *133*, 283–304.

Malhotra, P. K. (1999). Response of buildings to near-field pulse-like ground motions. *Earthquake Engineering and Structural Dynamics*, *28*, 1309–1326.

Musson, R. M. W. (2005). Intensity attenuation in the UK. *Journal of Seismology*, *9*, 73–86.

Oh, C. W. (2006). A new concept on tectonic correlation between Korea, China and Japan: Histories from the late Proterozoic to Cretaceous, *Gondwana Research*, *9*, 47–61.

Olsen, K. B. (2000). Site amplification in the Los Angeles basin from three-dimensional modeling of ground motion. *Bulletin of the Seismological Society of America*, *90*, S77–S94.

Papazachos, C., & Papaioannou, C. (1997). The macroseismic field of the Balkan area. *Journal of Seismology*, *1*, 181–201.

Pasolini, C., Albarello, D., Gasperini, P., D'Amico, V., & Lolli, B. (2008). The attenuation of seismic intensity in Italy. Part II: Modeling and validation. *Bulletin of the Seismological Society of America*, *98*, 692–708.

Reilly, W. I. (1962). Gravity and crustal thickness in New Zealand. *New Zealand Journal of Geology and Geophysics*, *5*, 228–233.

Roth, E. H., Wiens, D. A., & Zhao, D. (2000). An empirical relationship between seismic attenuation and velocity anomalies in the upper mantle. *Geophysical Research Letters*, *27*, 601–604.

Semblat, J. F., Kham, M., Parara, E., Bard, P. Y., Pitilakis, K., Makra, K., et al. (2005). Seismic wave amplification: Basin geometry vs soil layering. *Soil Dynamics and Earthquake Engineering*, *25*, 529–538.

Slejko, D., Peruzza, L., & Rebez, A. (1998). Seismic hazard maps of Italy. *Annals of Geophysics*, *41*, 183–214.

Snieder, R., & Şafak, E. (2006). Extracting the building response using seismic interferometry: Theory and application to the Millikan Library in Pasadena, California. *Bulletin of the Seismological Society of America*, *96*, 586–598.

Sokolov, V. Y., & Chernov, Y. K. (1998). On the correlation of seismic intensity with Fourier amplitude spectra. *Earthquake Spectra*, *14*, 679–694.

Sørensen, M. B., Stromeyer, D., & Grünthal, G. (2009). Attenuation of macroseismic intensity: A new relation for the Marmara Sea region, northwest Turkey. *Bulletin of the Seismological Society of America*, *99*, 538–553.

Stromeyer, D., & Grünthal, G. (2009). Attenuation relationship of macroseismic intensities in Central Europe. *Bulletin of the Seismological Society of America*, *99*, 554–565.

Szeliga, W., Hough, S., Martin, S., & Bilham, R. (2010). Intensity, magnitude, location, and attenuation in India for felt earthquakes since 1762. *Bulletin of the Seismological Society of America*, *100*, 570–584.

Tilford, N. R., Chandra, U., Amick, D. C., Moran, R., & Snider, F. (1985). Attenuation of intensities and effect of local site conditions on observed intensities during the Corinth, Greece, earthquakes of 24 and 25 February and 4 March 1981. *Bulletin of the Seismological Society of America*, *75*, 923–937.

Trifunac, M. D., & Brady, A. G. (1975). On the correlation of seismic intensity scales with the peaks of recorded strong ground motion. *Bulletin of the Seismological Society of America*, *65*, 139–162.

Trifunac, M. D., & Lee, V. W. (1989). Empirical models for scaling Fourier amplitude spectra of strong ground acceleration in terms of earthquake magnitude source to station distance, site intensity and recording site conditions. *Soil Dynamics and Earthquake Engineering*, *8*, 110–125.

Walsh, J. B. (1966). Seismic wave attenuation in rock due to friction. *Journal of Geophysical Research*, *71*, 2591–2599.

Yang, J., & Sato, T. (2000). Interpretation of seismic vertical amplification observed at an array site. *Bulletin of the Seismological Society of America*, *90*, 275–285.

Yin, A., & Nie, S. (1993). An indentation model for the North and South China collision and the development of the Tan-Lu and Honam fault systems, eastern Asia. *Tectonics*, *12*, 801–813.

Zhao, D., Huang, Z., Umino, N., Hasegawa, A., & Yoshida, T. (2011). Seismic imaging of the Amur-Okhotsk plate boundary zone in the Japan Sea. *Physics of the Earth and Planetary Interiors*, *188*, 82–95.

Zohar, M., & Marco, S. (2012). Re-estimating the epicenter of the 1927 Jericho earthquake using spatial distribution of intensity data. *Journal of Applied Geophysics*, *82*, 19–29.

(Received June 29, 2016, revised April 19, 2017, accepted May 16, 2017, Published online May 27, 2017)